Final Products of One-Electron Oxidation of Cyclic Dipeptides Containing Methionine Investigated by IRMPD Spectroscopy: Does the Free Radical Choose the Final Compound?

Yining Jiang, Suvasthika Indrajith, Ariel Francis Perez Mellor, Thomas Bürgi, Marc Lecouvey, Carine Clavaguéra, Enrico Bodo, Chantal Houée-Levin, E. Loire, Giel Berden, et al.

Final products of One-Electron Oxidation of Cyclic Dipeptides containing Methionine investigated by IRMPD Spectroscopy: does the Free Radical choose the Final compound?

Yining Jiang[1], Suvasthika Indrajith[1,2], Ariel Francis Perez Mellor[3], Thomas Bürgi [3] Marc Lecouvey[4], Carine Clavaguéra[1], Enrico Bodo[5], Chantal Houée-Levin[1], Estelle Loire[1], Giel Berden[6], Jos Oomens[6,7] and Debora Scuderi [1,]*

[1]Université Paris-Saclay, CNRS, Institut de Chimie Physique, UMR8000, 91405 Orsay, France.
[2]Stockholm University, Roslagstullsbacken 21 C, plan 4, Albano, Fysikum, 106 91 Stockholm, Sweden.
[3] Faculté des Sciences, Section de Chimie et Biologie, Département de Chimie Physique, Université de Genève, 30 Quai Ernest-Ansermet, CH-1211 Genève, Switzerland.
[4]Department of Chemistry, Université Sorbonne Paris Nord, CSPBAT, CNRS, UMR 7244, 1 rue de Chablis, Bobigny, F-93000, France.
[5]Departement of Chemistry, Università di Roma La Sapienza, P. Aldo Moro 5, 00185 Rome, Italy.
[6]Radboud University, Institute for Molecules and Materials, FELIX Laboratory, Toernooiveld 7, Nijmegen, 6525 ED, The Netherlands.
[7]Van't Hoff Institute for Molecular Sciences, University of Amsterdam, P.O. Box 94157, Amsterdam, 1090 GD, The Netherlands.

KEYWORDS. One-electron oxidation, γ-radiolysis, IRMPD spectroscopy, tandem mass spectrometry, cyclic peptides.

ABSTRACT

Reactive oxygen species (ROS) such as hydrogen peroxide (H_2O_2) and the hydroxyl radical ($^{\bullet}OH$) have specific functions in biological processes, while their uncontrolled production and reactivity are known to be determining factors in pathophysiology. Methionine (Met) residues act as endogenous antioxidants, when they are oxidized into methionine sulfoxide (MetSO), thus depleting ROS and protecting the protein.

We employed tandem mass spectrometry combined with IR Multiple Photon Dissociation Spectroscopy (IRMPD) to study the oxidation induced by OH radicals produced by gamma radiolysis on model cyclic dipeptides c(LMetLMet), c(LMetDMet), and c(GlyMet). Our aim was to characterize the geometries of the oxidized peptides in the gas phase and to understand the relationship between the structure of the 2-centre 3-electron (2c-3e) free radical formed in the first step of the oxidation process and the final compound. DFT calculations were performed to characterize the lowest energy structures of the final product of oxidation and to interpret the IR spectra.

Collision-induced dissociation tandem mass spectrometry (CID-MS^2) experiments of oxidized c(LMetLMet)H^+ and c(LMetDMet)H^+ led to the loss of one or two oxidized sulfenic acid molecules indicating that the addition of one or two oxygen atoms occurs on the sulfur atom of both methionine side chains and no sulfone formation was observed. The CID-MS^2 fragmentation mass spectrum of oxidized c(GlyMet)H^+ showed only the loss of one oxidized sulfenic acid molecule. Thus, the final products of oxidation are the same regardless of the structure of the precursor sulfur centered free radical.

INTRODUCTION

Reactive oxygens species (ROS) have special function in the biology of living organisms. While they are crucial signaling agents in various biological processes, essential for sustaining the life of cells, their uncontrolled production is generally considered to be an important factor in the pathophysiology of various states, including ischemia, atherosclerosis, heart failure and cancer[1]. ROS are produced in living cells by Fenton reaction[2] and/or enzymes such as NADPH oxidase. An imbalance of the equilibrium between the free radical formed during the oxidation process and

the antioxidant defense mechanisms leads to oxidative stress and a variety of critical biological molecules, including DNA and cellular proteins, are subjected to oxidative damage[3]. •OH, which is the most reactive oxygen species, is also generated by the radiolysis of water molecules according to the so-called indirect effect of ionizing radiation, involving hydrogen peroxide[4]. Gamma radiolysis can in this way mimic oxidative stress in cells.

Almost all peptide residues can be oxidized by OH radicals. Most of these oxidized residues are toxic. Two major exceptions are the sulfur containing residues (cysteine and methionine), which not only are very easily oxidized but can also be repaired by cellular machineries (thiol-disulfide cycles for the former and methionine sulfoxide reductases for the latter). Methionine (Met) residues are often considered as endogenous antioxidants that can detoxify the cell and protect crucial regions of proteins[5,6]. Other studies have also shown pro-oxidant properties thanks to intramolecular long-range electron transfer at the free radical level[7]. The condition under which Met can provide its antioxidant action is that the oxidation should produce methionine sulfoxide (MetSO) but no other species containing $-SO_2$ or $-SO_3$.

In this context, considerable efforts have been devoted to developing analytical strategies to detect oxidized Met residues (see[8] and references therein) and among them tandem mass spectrometry (MS/MS) is largely used, especially in combination with the electrospray ionization technique (ESI). [9]. Tandem mass spectrometry is a highly and efficient analytical tool, whose potential was impeded by the limited structural information which it can provide[10] . Tandem mass spectrometry combined with IRMPD spectroscopy has become a powerful tool for the characterization of molecular ion structures in the gas phase, allowing the localization of the post-translational modifications and giving information on their nature [8].

IRMPD spectroscopy experiments need to be performed with free electrons lasers (FEL) at the FELIX (Free Electron Laser for Infrared eXperiment) laboratory in the Netherlands[11] or at the CLIO (Centre Laser Infrarouge d'Orsay) facility in France[12], which are characterized by a high power and IR tunability.

In previous studies[13] performed at the CLIO facility in Orsay, we have investigated the oxidation products formed from linear dipeptides containing methionine by tandem mass spectrometry and IRMPD spectroscopy. The sulfoxide signature has been recognized near 1000 cm^{-1} in the IRMPD spectrum of the oxidation products of dipeptides such as Val-Met, Tyr-Met and Met-Met.

In Lys-Met, we were able to unravel the mechanism involved in the formation of the sulfoxide[14]. In the dipeptides Trp-Met and Met-Trp we were able to show the formation of a sulfoxide on both peptides and on the latter one we shown evidence of the oxidation occurring also on the aromatic ring of Trp[15].

In the present work, our aim is to shed light on the mechanism of these damaging events, by investigating in more detail the role of the neighboring groups on the final products of the oxidation of model cyclic dipeptides containing methionine (**Figure 1**). We further aim to understand the relationship between the 2-centre 3-electron free radical formed in the first step of the oxidation process and the final compound. Few studies have attempted to obtain a complete picture of Met oxidation, *i.e.*, from the free radicals to the final products[16]. The chemical properties of these free radicals and especially the relationship between their structure and the final products are not yet completely known.

In the past few decades, mechanistic investigations by pulse radiolysis have highlighted the complexity of solution-phase one-electron oxidation of methionine and polypeptides by OH

radicals[17,18]. Several Met free radicals can be formed depending on the geometry of the peptide and the neighboring residues, in particular, 2-center 3-electron bonded free radicals (2c-3e) have been discovered in which the odd electron of sulfur makes a bond with any atom possessing a lone pair, as confirmed by quantum-chemical calculations[16,19–23]. The sulfur radical cations formed as transient species are stabilized due to interaction with the oxygen and nitrogen atoms of the peptide bond [20]. In this way the formation of a sulfoxide is possible. Cyclic peptides are an interesting class of molecules as models for the interior of (linear) proteins, where terminal groups are absent, like calmodulin[6], a protein with adjacent methionine residues. c(LMetDMet) serves as a better model for calmodulin than c(LMetLMet) because the methionine lateral chains are pointing in opposite directions due to the cis configuration of the peptide bond in cyclic peptides. Various previous studies have employed IRMPD spectroscopy to efficiently characterize the structures of cyclic peptides in the gas phase[24–27].

METHODS

Products. The peptides were synthesized in the group of Prof. Marc Lecouvey at Sorbonne University Paris Nord and used as received. To synthesize the different peptidic targets, classical methodologies were used[28,29]. A detailed description of the synthesis is reported in **Figure S1** and **S2.** Nitrous oxide with a global purity of 99.998% was purchased by ALPHA GAZ.

Gamma Irradiation. To perform γ-irradiations the panoramic ^{60}Co γ-source IL60PL Cis-Bio International (France) in the Paris-Saclay University (Orsay, France) has been employed. The dose rate was determined by Fricke dosimetry[30]. Before the irradiation, performed at room temperature, the samples were purged under a N_2O atmosphere for 30 min. The well-known method of

scavengers[31] allows a quantitative production of free radicals by stationary γ-radiolysis according to the following reactions. The chosen oxidant species was the hydroxyl radical •OH produced by γ- radiolysis of N_2O-saturated aqueous solutions:

$$H_2O \rightarrow {}^{\bullet}OH, H^{\bullet}, e^-_{aq}, H_2, H_2O_2, H^+, OH^- \quad (1)$$

$$e^-_{aq} + N_2O + H_2O \rightarrow {}^{\bullet}OH + OH^- + N_2 \quad (2)$$

The radiation chemical yield (G) is equal to 0.55 μmol J^{-1} (equations 1 and 2)[31]. H atoms are also created in much lower yield (0.05 μmol J^{-1}), leading to the desulfuration of methionine. The H_2O_2 yield is also lower (0.07 μmol J^{-1}).

Infrared absorption spectroscopy. The infrared absorption spectra of c(LMetLMet), c(LMetDMet) and c(GlyLMet) were investigated in different environments: pure powder, a KBr pellet containing the powder at ~1%, and a DMSO-d6 solution. We used Attenuated Total Reflectance (ATR) for pure powder measurements, while for KBr and DMSO-d6 solution, we measured the absorbance in transmission. For the latter, we use pure KBr pellets and pure solvent as a reference spectrum. In all cases, the resolution is set at 4 cm^{-1}, and 100 scans were collected.

MS operations and IRMPD spectroscopy. IRMPD spectroscopy experiments were performed both at the FELIX Laboratory in Nijmegen (The Netherlands)[32] and at the CLIO Facility in Orsay (France)[33]. IRMPD experiments at the CLIO Facility have been performed in the 1000−3700 cm^{-1} spectral range. Infrared ion spectra were recorded using the 7 T hybrid FT-ICR mass spectrometer (APEX-Qe, Bruker) coupled to the CLIO beamline or to the OPO/OPA system (LaserVision). This

experimental setup has been previously described in detail[34]. To perform the IRMPD experiments mass-selected ions were stored and irradiated for 1 to 4 seconds with the IR-FEL (corresponding to 25-100 pulses) or OPO/OPA (10-40 pulses) light in the frequency range of interest. At 44 MeV electron energy, the time-averaged CLIO laser power is between 0.5 and 1.2 W. The OPO/OPA power is between 0.1-0.2 W. The bandwidth at room temperature is about 10 cm^{-1} in the IRMPD spectra. We used a CO_2 laser synchronized with the CLIO FEL or the OPO/OPA system for few tens of milliseconds at the beginning of the irradiation period to improve the ion fragmentation (Universal Laser System, 10 W, continuous wave operation, wavelength 10.6 μm).

Room temperature experiments in the fingerprint region, 600-2100 cm^{-1}, were also performed at the FELIX laboratory. The FEL was coupled to a Bruker AmaZon ETD quadrupole ion trap mass spectrometer, which was modified to have optical access to the ion trapping region as ~~is~~ described in detail elsewhere[35]. The IR frequency was calibrated using a grating spectrometer. Protonated ions were generated from solution by ESI, mass-to-charge isolated in the trap, and irradiated with a single infrared laser pulse from the FEL (40-100 mJ per pulse, bandwidth 0.4% of the IR frequency) to induce wavelength-dependent IRMPD. Precursor and fragment ion intensities were determined from 6 averaged mass spectra at each IR frequency.

The IRMPD spectra are obtained by recording the photofragmentation yield, $R = -\ln[I_p/(I_p+\Sigma I_f)]$ as a function of the wavenumber of the IR radiation, with I_p and I_f the precursor and fragment ion intensity. The IR yield has been linearly corrected for the frequency-dependent variation of the laser pulse energy[36].

Computational details. To evaluate the effect of the keto or enol form of the peptide bond on the IR spectra, we carried out a theoretical investigation on neutral c(GlyLMet). To this end, we have explored the conformational landscape of three possible ring shapes, namely, keto, enol01, and

enol02. In this case, we take advantage of the conformational search tool implemented in the Maestro program. The mixed torsional/low-mode sampling method was used. The OPLS-2005 force field was employed with an energy window for saving structures fixed at 20 kJ/mol. This approach provides 27, 44, and 20 initial structures for each ring shape, keto, enol01, and enol02. Further geometry optimization and frequency calculation have been performed at the B3LYP/6-311++g(d,p)/PCM(DMSO) level. Frequency-dependent scaling factors 0.977 (if ~ν< 2000), 0.957 (if 2000 <ν> 3400) and 0.953 (if 3400 < ν) were used to adequately correct for anharmonicity effects and basis set incompleteness. Stick spectra were convolved using a Lorentzian line shape with 8 cm^{-1} of full width at half maximum (FWHM).

Spectral assignment of protonated cyclic dipeptides has been achieved by comparing experimental IRMPD spectra to calculated vibrational spectra.

The conformer sampling of the cyclic dipeptides has been carried out using the iterative metadynamics sampling and genetic crossover (iMTD-GC) method implemented in the Conformer Rotamer Ensemble Sampling Tool (CREST) program[37,38]. The sampling has included additional geometry optimization of the final conformer ensemble. During this workflow, the calculations of the conformer energies have been based on the semi-empirical extended tight-binding method (GFN2-xTB)[39]. Thus, an ensemble of conformers within 40 kJ/mol of the minimum energy conformer has been generated and a clustering algorithm using principal component analysis has been used to select the 100 most representative conformers.

In order to get a better energy estimation, the geometries of characteristic conformers of dipeptides and their oxidized forms were re-optimized at the B3LYP/6-311G(d) level of the theory. The IR absorption spectra were computed at the same level of theory using a Lorentzian convolution with a 20 cm^{-1} FWHM. To account for anharmonicity, the calculated harmonic frequencies were

uniformly scaled by 0.96, which turned out to improve the agreement between calculated and measured absorptions. However, the frequencies associated with the sulfur atom were left unscaled, which complied with previous evidence[40–42]. All DFT static calculations were performed with the Gaussian 16 package[43]. Furthermore, single-point energy calculations were computed for the lowest-energies conformers at the DLPNO-CCSD(T)/cc-pvTZ level of theory using the ORCA program package[44]. These electronic energies were used in combination with DFT thermal corrections to compute relative Gibbs energies.

RESULTS & DISCUSSION

MS and MS^2-CID spectra. The mass spectra (MS) of the samples containing non-irradiated dipeptides and dipeptides oxidized by OH radicals are reported in **Figure 2**. The most intense peaks at *m/z* 263 and 189 in the MS of the non-irradiated c(MetMet) and c(GlyMet), respectively, are attributed to the protonated dipeptides.

Singly (M+16) and doubly (M+32) oxidized products, *m/z* 279 and 295, were found for c(LMetLMet) and c(LMetDMet) (**Figure 2.a and b**), while only the single-oxidation product (M+16) at (*m/z* 205) was observed for c(GlyMet) (**Figure 2.c**). For c(LMetLMet) and c(LMetDMet), the product of dehydrogenation at *m/z* 261 was also observed after radiolysis, as already observed in the case of linear Val-Met and Met-Val dipeptides[12]. A peak at *m/z* 214 was observed in the spectrum of c(GlyMet), corresponding to instrumental contamination (n-butyl benzenesulfonamide, n-BBS).

To characterize the final oxidation products, collision induced dissociation (CID-MS^2) of mass selected products was performed. The identification of the main fragments for each oxidation

product is summarized in **Tables S1** c(LMetLMet)H^+, **S2** c(LMetDMet)H^+ and **S3** c(GlyMet)H^+ in the supporting information.

The CID-MS^2 fragmentation mass spectra (**Figure S3-5**) of protonated dipeptides are characterized by the loss of sulfenic acid (-$HSCH_3$) from the methionine side chain. In the case of c(LMetLMet)H^+ and c(LMetDMet)H^+ a peak at *m/z* 167 was observed as well, which is attributed to the loss of two sulfenic acid molecules.

The MS^2-CID fragmentation of electrosprayed mass selected oxidation products of c(LMetLMet)H^+ and c(LMetDMet)H^+ show the loss of one oxidized sulfenic acid molecule (-$HSCH_3$+O) indicating that the oxidation can occur on the sulfur atom of both methionine side chains. No sulfone formation was observed. As expected, the CID-MS^2 fragmentation mass spectra of oxidized c(GlyMet)H^+ shows only the loss of one oxidized sulfenic acid molecule.

Thus, the final products of oxidation are the same for c(LMetLMet)H^+ and c(LMetDMet)H^+. In addition, there is no clear difference in the final yields of oxidation products. Stabilization of the radical cation $>S\bullet^+$ by the formation of either $(S\therefore S)^+$ or $(S\therefore N)^+$[16] does not impact the nature of the final products.

IR absorption spectra. In order to determine whether a single structure or a mixture of multiple structures from different families (for instance, keto-enol) are present in the powder and in the solution, we recorded the IR absorption spectra of pure powder, a KBr pellet containing the powder at ~1%, and in DMSO-d6 solution for the three cyclic peptides. We simulated the IR absorbance spectrum for the c(GlyMet) system (the simplest cyclic system) at the B3LYP/6-311++g(d,p)/PCM(DMSO) level of the theory. This spectrum (**Figure S6**) shows that there is a clear difference in the C=O stretch region between the keto and enol forms. The keto spectrum has a single band around 1662 cm^{-1} due to the two CO stretches, while the enols have a similar peak,

with an additional band due to the formation of the enol group at 1710 cm^{-1}. The latter is a sign of the presence of the enolic form.

In c(GlyMet), the keto form is more stable than the enol form by 96 kJ/mol. The sign of the presence of the enol form is missing from the experimental IR absorption spectra of c(GlyMet) (**Figure S7)**, which indicates that the system remains in keto form. The presence of keto form and absence of enol can also be confirmed in the c(LMetLMet) and c(LMetDMet) spectra **(Figure S8**) due to a single band in the C=O stretching region.

IRMPD spectra. The IRMPD spectra of protonated c(LMetLMet), c(LMetDMet), c(GlyMet) and of their corresponding oxo-forms are reported in **Figure 3**. Both spectra of non-oxidized c(MetMet)H^+ and of c(GlyMet)H^+ show similar features in the 800-3700 cm^{-1} energy range. For the protonated cyclic peptides, the ν(CO) stretch region is characterized by two features (a sharp peak and a broad band) located at 1755-1665 cm^{-1} in the spectrum of c(LMetLMet)H^+ and at 1751-1676 and 1763-1639 cm^{-1} for c(LMetDMet)H^+ and c(GlyMet)H^+. These bands are typical of an amide I vibrational mode in DKP rings[25,26]. The NH-bending range displays two bands at 1487 and 1436 cm^{-1} in the spectrum of c(LMetLMet)H^+, whose counterpart is found at 1495 and 1435 cm^{-1} for c(LMetDMet)H^+ and 1470 and 1425 cm^{-1} for c(GlyMet)H^+. The region of the β(OH) and aliphatic β(CH) bending modes shows two bands at 1315 and 1219 cm^{-1} for c(LMetLMet)H^+. They are observed at 1317, 1278 cm^{-1} and 1218 cm^{-1} for c(LMetDMet)H^+. An intense band at 1301 cm^{-1} with some satellite peaks to the red is observed in the spectrum of c(GlyMet)H^+.

The high frequency region is characterized by features that are similar for the three cyclic dipeptides: a broad band observed from 2600 to 3200 cm^{-1}, an intense and a narrow peak ~~is~~ observed at 2941 cm^{-1} for c(LMetLMet)H^+, whose counterpart is found at 2942 cm^{-1} for

c(LMetDMet)H^+. This intense band is not observed in the IRMPD spectrum of c(GlyMet)H^+. In the region of the NH-stretch modes, intense peaks are also observed at 3423 and 3416 cm^{-1} for c(LMetLMet)H^+ and c(LMetDMet)H^+, respectively. This band is red shifted at 3389 cm^{-1} for c(GlyMet)H^+. In the ν(OH) region, c(LMetLMet)H^+ shows a weak band at 3585 cm^{-1}. Two weak bands are observed at 3494 and 3567 cm^{-1} for c(LMetDMet)H^+ and 3564 and 3598 cm^{-1} for c(GlyMet)H^+. IRMPD spectra of the oxo-forms of cyclic peptides show some differences compared to those of the native peptides, especially in relative band intensities and in the fingerprint region. We have already shown that the sulfoxide group exhibits a specific band around 900-1000 cm^{-1} [14]. ν(SO) has been observed at 869 cm^{-1} in the IRMPD spectrum of c[(LMetLMet)(O)H]$^+$, whose counterpart is found at 871 cm^{-1} in the IRMPD spectrum of c[(LMetDMet)(O)H]$^+$ and 881 cm^{-1} in the IRMPD spectrum of c(GlyMet)(O)H^+.

Theoretical Results and Band Assignment. The nomenclature used for the molecules is shown in **Figure 1**. A subscript p is employed to indicate the peptide bond atoms on the protonated moiety. C_α, C_β, or C_γ indicates the carbon atom position relative to the peptide bond. Different forms of cyclic peptides have been extensively explored. Among them, the ketone forms show the lowest calculated energy (all structures explored with corresponding IR spectra and calculated energies are displayed in **Figure S9-42** and **Tables S4-9**). The calculated structure for c(LMetLMet) and its oxo-form referred to as LL and LLO; c(LMetDMet) and its oxo-form referred to as LD and LDO; c(GlyMet) and its oxo-form referred to as GM and GMO. The tautomerization type of the structures (keto for ketone forms, enol for enol forms, iminol for iminol

forms, cycl for cyclic structures, and open for open structures) and an energetic ranking number is also indicated in the structure nomenclature for the sake of clarity.

For the non-oxidized forms, two protonation sites can be considered: the amide oxygen or nitrogen atoms. For c(LMetLMet), c(LMetDMet) and c(GlyMet), the most stable structures correspond to protonation at the amide oxygen atom, as already observed for similar systems investigated by IRMPD spectroscopy[25,26]. The amide bond remains planar or quasi planar. The DKP structure is puckered in a flattened boat structure or puckered with a puckering angle from 20 to 50°. Structures characterized by a hydrogen bond between the protonated carbonyl group and the sulfur atom of the methionine side chain show the methionine side chain in the plane of the DKP ring, while in the structures without hydrogen bond the methionine side chain is close to 90° compared to the DKP ring.

Oxidation of methionine to methionine sulfoxide derivatives increases the proton affinity of the sulfur atom[45,46].

As a consequence, the lowest-energy conformers of the oxidized cyclic peptides are in a keto form and are protonated on the sulfoxide group. Protonation on the amide oxygen leads to conformers at higher energy, depending on the hydrogen bond network stabilizing the structure. These conformers can be formed under our experimental conditions during the gamma radiolysis in solution or during the electrospray process used to generate the gas-phase ions depending on the internal energies of the ions[47].

The vibrational bands in the IRMPD spectrum are sequentially labeled alphabetically to facilitate the comparison with the calculated ones. Relative Gibbs energies are provided at the DFT level, and also, in parenthesis, by incorporating DLPNO-CCSD(T) electronic energies in **Figure 4 to 9**.

Considering this last approximation and as no significant differences have been found between the two sets of relative Gibbs energies, only DFT energies are reported in the following sections.

c(LMetLMet)H$^+$ and [c(LMetLMet)(O)H]$^+$. The experimental IRMPD spectrum of c(LMetLMet)H$^+$ and the simulated IR spectra for **LLketo01**, **LLketo02** and **LLketo04** geometries are reported in **Figure 4** together with the corresponding calculated geometries. The calculated IR spectra for the three keto forms show the best agreement with the IRMPD one and allow all peaks observed to be assigned. **LLketo01**, **LLketo02** and **LLketo04** are all characterized by protonation on the amide oxygen. In **LLketo01**, the proton is involved in a hydrogen bond with the sulfur atom. This conformer is also stabilized by an NH…..S interaction. Its calculated IR spectrum shows good agreement with the IRMPD one for the major bands from **B** to **I**. **LLketo02**, which shows a more puckering boat structure, is 19.7 kJ/mol higher in energy compared to **LLketo01** and allows for a better assignment of band **A**. Its structure is stabilized by two non-covalent interactions: an NH…..S interaction and a COH….S one. The position of band **F** is predicted slightly towards the red in **LLketo02** and allows to justify the broad band observed in the IRMPD spectrum. Meanwhile, it is necessary to populate a third conformation **LLketo04** found at 31.3 kJ/mol to justify band **J** in the hydrogen stretching region Kinetic trapping could explain the presence of thermodynamically disfavored species[26,48,49]. The population of different conformers **LLketo01, LLketo02** and **LLketo04** justify the broad bands **C**, **D, E** and **F** observed in the IRMPD spectrum of c(LMetLMet)H$^+$.

Tentative assignments of IRMPD spectral bands of c(LMetLMet)H$^+$ are detailed in **Table 1**.

We have calculated the IR spectra of other possible families for c(LMetLMet)H^+. Their structures and the IR spectra are reported in **Figures S9-14**. These structures can be ruled out on energetic criteria.

A comparison of the calculated IR spectra of the most stable geometries of [c(LMetLMet)(O)H]$^+$, **LLOketo01**, **LLOketo02**, **LLOketo03** and **LLOketo12,** with the experimental IRMPD one is reported in **Figure5**. **LLOketo01** is the most stable conformer for [c(LMetLMet)(O)H]$^+$, stabilized by a network of two hydrogen bonds. Protonation occurs on the oxygen of the sulfoxide group, as in **LLOketo02** and **LLOketo03.** The protonated sulfoxide group is involved in a hydrogen bond with the carbonyl group S=O-H…..O=C . **LLOketo01** is also stabilized by an NH…..S interaction. The amide bond remains planar. The DKP structure is slightly puckered in a flattened boat structure. **LLOketo02** is only 2.1 kJ/mol higher in energy than **LLOketo01**. The DKP structure adopts a flattened boat structure. **LLOketo03** is 3.9 kJ/mol higher in energy than **LLOketo01** and characterized by a hydrogen bond between the amide NH group and the non-oxidized sulfur atom. It shows a boat structure. Finally, **LLOketo12** is at 33 kJ/mol, protonated on the carbonyl moiety, and stabilized by a hydrogen bond between the amide N_pH group and the S=O group.

A tentative assignment of the experimental bands is reported in **Table 2.** In the fingerprint region, band **A** at 869 cm^{-1} is assigned to the S=O stretch combined with SCH and SOH bending character. This band is diagnostic of the sulfoxide formation during the oxidation process and it is not observed in the IRMPD spectrum of the protonated non-oxidized dipeptide.

A very intense band is predicted in the calculated IR spectra of **LLOketo02** and **LLOketo12** at 2337 and 2530 cm^{-1}**,** respectively, which is due to stretching of the OH of the protonated S=O group.

c(LMetDMet)H^+ and [c(LMetDMet)(O)H]$^+$. A comparison of the calculated IR spectra of the most stable geometries of c(LMetDMet)H^+, **LDketo01**, **LDketo02** and **LDketo06,** with the experimental IRMPD spectrum is shown in **Figure 6**. As observed for c(LMetLMet)H^+, all three structures are keto forms with protonation on the amide oxygen. A combination of the calculated spectra for these three structures can explain the ensemble of features observed in the IRMPD spectrum of c(LMetDMet)H^+. The most stable structure **LDketo01** features a proton shared between the amide oxygen and the sulfur atom, which stabilizes the structure. The DKP ring is in a slightly twisted boat structure. **LDketo02** and **LDketo06** are required to account for the presence of the bands **L** and **M**. The band predicted at 1682 cm^{-1} for **LDketo06** is slightly blue-shifted compared to its counterparts in the other two structures, and the contribution of this band accounts for the broadening of band **G** in the IRMPD spectrum. Both **LDketo02** and **LDketo06** are stabilized by a non-covalent N_pH…..S interaction **LDketo02** possesses a quasi-planar structure while **LDketo02** presents a flattened boat DKP ring.

The band assignments of c(LMetDMet)H^+ are detailed in **Table 3**.

A comparison of the IRMPD spectrum of the oxo-form of c(LMetDMet)H with the simulated spectra of the lowest energy structures **LDOketo01**, **LDOketo02**, **LDOketo04**, **LDOketo06** and **LDOimin01** is displayed in **Figure 7**. **LDOketo01** is the lowest-energy conformer and is protonated on the sulfoxide oxygen, while **LDOketo02**, **LDOketo04** and **LDOketo06** are protonated on the amide oxygen. Finally, **LDOimin01** is protonated on the iminol oxygen. The most stable structure **LDOketo01** presents a flattened boat form, while **LDOketo02,** is characterized by a planar structure. **LDOketo04** shows a puckering boat structure **LDOketo06** (+14.9 kJ/mol) shows a planar structure with one side chain pointing directly above the DKP ring. Finally, **LDOimin01** is in a slightly puckered boat structure.

LDOketo01 is stabilized by a hydrogen bond between the protonated sulfoxide group and the amide oxygen. Both **LDOketo02** and **LDOketo04** feature a shared proton between the sulfoxide and amide oxygen atoms. **LDOketo06** has an amide nitrogen involved in a hydrogen bond with the sulfoxide group N_pH.....O=S. No particular intra-molecular interaction is seen in **LDOimin01**. **LDOketo01** owns a prominent band centered at 1298 cm^{-1} that can be associated with experimental band **D**. Bands **H**, **I**, **J** and **K** observed in the IRMPD spectrum of $[c(LMetDMet)(O)H]^+$ also find a counterpart in the calculated IR spectrum of **LDOketo01**. A contribution of **LDOketo02** and **LDOketo04** are required for explaining the presence of the intense band **A** observed in the IRMPD spectrum. The population of **LDOketo06** and **LDOimin01** can justify the presence of the weak bands **M** and **N** in the NH/OH stretching region.

Band assignment for $[c(LMetDMet)(O)H]^+$ is reported in **Table 4**. In the fingerprint region, bands **A** and **B** are related to the diagnostic SO stretching mode. The prominent band **A**, centered at 871 cm^{-1}, is assigned to the stretching modes of SO and CC bonds, along with the bending of CH_2 and CH_3. The asymmetric band **B** at 1074 cm^{-1} is attributed to the SO stretching mode accompanied by the CH_2 and CH_3 bending modes.

c(GlyMet)H$^+$ and [c(GlyMet)(O)H]$^+$. A comparison of the IRMPD spectrum of $c(GlyMet)H^+$ with the calculated IR spectra of the lowest energies keto form **GMketo01**, **GMketo02**, **GMketo03** and **GMketo05** is shown in **Figure 8**. **GMketo01** is the most stable conformer of $c(GlyMet)H^+$ and allows to justify most of the experimental features observed in the IRMPD spectrum: especially bands **B-H** and **J-K**. The calculated IR spectra of **GMketo01, GMketo02** and **GMketo03** are quite similar. **GMketo02** and **GMketo03** show better agreement with band **A** than **GMketo01**. **GMketo02** and **GMketo03** are at 8.2 and 10.9 kJ/mol higher in energy compared

to **GMketo01**, respectively. It is still necessary to assume population of a fourth conformer **GMketo05**, lying at 19.6 kJ/mol higher in energy compared to **GMketo01**, to justify the bands **I** and **L** in the high frequency region. The protonation site is always on the amide oxygen for these structures. Other possible families have also been investigated (**Figure S33-36**, energies are listed in **Table S8**), but the results prove that keto forms are generally at lower energy levels and were close enough to explain the experimental spectrum.

Detailed band positions along with a concise description of the assigned vibrational modes for c(GlyMet)H^+ are listed in **Table 5**.

The IRMPD spectrum of [c(GlyMet)(O)]H^+ is compared with the predicted spectra for the **GMOketo01**, **GMOketo02** and **GMOketo03** in **Figure 9**. **GMOketo01**, conformer is the lowest in energy. It is protonated on the sulfoxide group. The protonation site of **GMOketo02** and **GMOketo03** is on the amide oxygen. **GMOketo01** is stabilized by a hydrogen bond with the carbonyl group S=O-H…..O=C and it shows in a flattened DKP structure with the amide group mildly twisted by the S=OH…..O interaction. It provides a general match of most of the spectral features. However, in order to justify all the IR absorption peaks observed in the IRMPD spectrum, we should admit that the following also populate in our experimental conditions: **GMOketo02** to justify the band **M** and **GMOketo03** for a better description of the band **N**. **GMOketo02** and **GMOketo03** lie 22.3 and 42.2 kJ/mol higher than **GMOketo01**, respectively. **GMOketo02** displays in a puckered boat structure, whereas the DKP ring structure of **GMOketo03** shows a flat character. We have extensively searched the existence of other families in the gas phase (**Figure S37-42**, relative free energies are listed in **Table S9**).

A tentative assignment of IRMPD features of [c(GlyMet)(O)]H^+ is proposed in **Table 6**. Diagnostic band for the formation of the sulfoxide is observed in the fingerprint region. The band **A** (881 cm^{-1}) is associated with a combination of SOH bending, SO and CC stretching modes. The intense bands predicted in **GMOketo03** and **GMOketo01** are assigned to N_pH stretching (2678 cm^{-1}) and OH stretching of the protonated S=O group (2763 cm^{-1}), respectively.

CONCLUSIONS

We studied the one-electron oxidation of cyclic methionine dipeptides by OH free radicals produced by gamma radiolysis. The first step of oxidation, *i.e.* the formation of the methionine free radicals has been studied some years ago by pulse radiolysis[17,18]. The authors demonstrated that the c(LMetLMet) isomer led to (S∴S) 2c-3e free radicals due to the proximity of the two sulfur atoms, while the c(LMetDMet) isomer formed (S∴N) 2c-3e free radicals. Our aim was to elucidate the fate of these two free radicals, which is still unknown. Our studies also gave elements to predict the reactivity of these free radicals. The final products were mass-isolated in the gas phase. CID-MS^2 tandem mass spectrometry and IRMPD spectroscopy have been performed. DFT calculations have been performed to explore their chemical structures in the gas phase and for vibrational band assignment.

Oxidation of both c(MetMet) peptides induced the formation of one or two sulfoxide groups on each sulfur atom. Oxidation of c(GlyMet) led only to one sulfoxide group. No sulfone has been detected. In addition, loss of dihydrogen was observed leading to a C=C double bond in the methionine side chain, due to the attack of OH radicals to the carbon atom adjacent to sulfur (formation of the so-called α–S free radical)[52]. These results are similar to those observed for e.g.

Met-Val and Val-Met peptides[53] . They demonstrate that both 2c-3e free radicals have the same fate, disproportionation plus hydration to give sulfoxide. A proposed mechanism for the one-electron oxidation of cyclic methionine dipeptide c(MetMet) is displayed in **Figure 10**. When hydroxyl-induced oxidation occurs, the initial cyclic dipeptide c(MetMet) (**a**) undergoes two possible pathways: H-atom abstraction or addition of OH radical. They are in competition with each other. The first pathway leads to the formation of α–S free radicals (**d**) and (**e**) by removing one hydrogen atom from the α–S position of (**a**). Disproportionation of (**d**) and (**e**) leads to (**a**) and the product with a C=C double bond (**i**) by the loss of H_2. In the second pathway, the thioether group of (**a**) is attacked by OH radical to form hydroxysulfuranyl radicals (**b**) which are highly unstable and decompose rapidly to S-centered radical cations (**c**). Three possible 2c-3e free radicals (**f**)-(**h**) can be formed through intramolecular or intermolecular stabilizations with a reactive site owing an electron lone pair. Hydration and disproportion of 2c-3e free radicals give rise to the formation of sulfoxide product c(MetMetSO) (**j**). The amount of sulfoxide formed in both c(LMetLMet) and c(LMetDMet) are quite similar and low (ca.5 %). The same amount of sulfoxide is observed for c(GlyMet). In addition, the similar yield of sulfoxide shows that the chirality of S-containing side chains in cyclic methionine dipeptides has no impact on the production of the final product.

IRMPD spectroscopy and DFT calculations allowed us to identify the chemical structures of the final products in the gas phase. In particular, we have shown that the cyclic dipeptides adopt a keto form in the gas phase, except for c(LMetDMet), where an iminol isomer can also be populated in our experimental conditions. IRMPD spectra are well reproduced by the calculated IR absorption spectra of the lowest energy isomers.

The non-oxidized dipeptides are protonated on the amide oxygen. Oxidation leads to the increase of the proton affinity of the sulfoxide group. In the oxidized cyclic dipeptides, the protonation site is the sulfoxide group. Structures with the protonation of the amide oxygen, at higher energy are also populated under our experimental conditions. IR spectra performed on the powders or on the solution showed that the dipeptides adopt a keto form of the DKP ring in the solid state or in solution before oxidation. Structures at higher energies are likely formed during the gamma radiolysis or are due to kinetic trapping in the electrospray source.

ASSOCIATED CONTENT

Supporting information

The supporting information is available free of charge via the internet at xxx.com

A detailed description of the synthesis process of cyclic peptides; the CID-MS^2 fragmentation mass spectra of protonated cyclic dipeptides and their oxidation products with the assignments of the observed peaks; experimental and simulated infrared absorption spectra in different environments (pure powder, KBr powder, DMSO-d6 solution); and geometries of the B3LYP/6-311g(d)-optimized stable conformers of protonated cyclic dipeptides and their oxidized forms, along with their calculated spectra and detailed structural information.

AUTHOR INFORMATION

Corresponding Author

*Debora Scuderi

Université Paris-Saclay, CNRS, Institut de Chimie Physique, UMR8000, 91405 Orsay, France.

E-mail: debora.scuderi@universite-paris-saclay.fr; Phone: +33 1 69 15 75 74.

ACKNOWLEDGMENT

This research was fund by the EU Horizon 2020 Programme (EU_FT-ICR_MS) under grant agreement No 731077. Financial support from the French National network INFRANALYTICS (FR 3624 CNRS) for conducting the research is gratefully acknowledged. The research leading to these results has received funding from LASERLAB-EUROPE (grant agreement no. 871124, European Union's Horizon 2020 research and innovation programme). We gratefully acknowledge the Nederlandse Organisatie voor Wetenschappelijk Onderzoek (NWO) for the support experiments performed at the FELIX Laboratory.

The mass spectrometry platform SMAS at the Institut de Chimie Physique (ICP) in Paris-Saclay University, J.M. Ortega and B. Redlich are gratefully acknowledged. We also thank the CLIO and FELIX facilities and the technical staffs, in particular Nicolas Jestin, Victor Claessen, Marije Barel, Wouter Stumpel and Bryan Willemsen for their efficient assistance during the IRMPD experiments. DS thanks Erna Gouwens from FELIX office for her assistance.

ABBREVIATIONS

IRMPD. Infrared multiple photon dissociation; ROS, Reactive oxygen species; CID, collision induced dissociation; MS^2 or MS/MS, tandem mass spectrometry; PTMs, post translational modifications; ESI, electrospray ionization; FEL, Free electron laser.

REFERENCES

(1) Grune, T.; Jung, T.; Merker, K.; Davies, K. J. A. Decreased Proteolysis Caused by Protein Aggregates, Inclusion Bodies, Plaques, Lipofuscin, Ceroid, and "aggresomes" during Oxidative Stress, Aging, and Disease. *Int. J. Biochem. Cell Biol.* **2004**, *36* (12), 2519–2530.

(2) Halliwell, B.; Cross, C. E. Oxygen-Derived Species: Their Relation to Human Disease and Environmental Stress. *Environ. Health Perspect.* **1994**, *102* (Suppl 10), 5–12.

(3) Winterbourn, C. C. Reconciling the Chemistry and Biology of Reactive Oxygen Species. *Nat. Chem. Biol.* **2008**, *4* (5), 278–286.

(4) Wojcik, A.; Bochenek, A.; Lankoff, A.; Lisowska, H.; Padjas, A.; Szumiel, I.; von Sonntag, C.; Obe, G. DNA Interstrand Crosslinks Are Induced in Cells Prelabelled with 5-Bromo-2′-Deoxyuridine and Exposed to UVC Radiation. *J. Photochem. Photobiol. B* **2006**, *84* (1), 15–20.

(5) Levine, R. L.; Berlett, B. S.; Moskovitz, J.; Mosoni, L.; Stadtman, E. R. Methionine Residues May Protect Proteins from Critical Oxidative Damage. *Mech. Ageing Dev.* **1999**, *107* (3), 323–332.

(6) Nauser, T.; Jacoby, M.; Koppenol, W. H.; Squier, T. C.; Schöneich, C. Calmodulin Methionine Residues Are Targets for One-Electron Oxidation by Hydroxyl Radicals: Formation of S∴N Three-Electron Bonded Radical Complexes. *Chem. Commun.* **2005**, No. 5, 587–589.

(7) Mozziconacci, O.; Mirkowski, J.; Rusconi, F.; Kciuk, G.; Wisniowski, P. B.; Bobrowski, K.; Houée-Levin, C. Methionine Residue Acts as a Prooxidant in the •OH-Induced Oxidation of Enkephalins. *J. Phys. Chem. B* **2012**, *116* (41), 12460–12472.

(8) Maitre, P.; Scuderi, D.; Corinti, D.; Chiavarino, B.; Crestoni, M. E.; Fornarini, S. Applications of Infrared Multiple Photon Dissociation (IRMPD) to the Detection of Posttranslational Modifications. *Chem. Rev.* **2020**, *120* (7), 3261–3295.

(9) Whitehouse, C. M.; Dreyer, R. N.; Yamashita, M.; Fenn, J. B. Electrospray Interface for Liquid Chromatographs and Mass Spectrometers. *Anal. Chem.* **1985**, *57* (3), 675–679.

(10) Bridgewater, J. D.; Srikanth, R.; Lim, J.; Vachet, R. W. The Effect of Histidine Oxidation on the Dissociation Patterns of Peptide Ions. *J. Am. Soc. Mass Spectrom.* **2007**, *18* (3), 553–562.

(11) Oomens, J.; van Roij, A. J. A.; Meijer, G.; von Helden, G. Gas-Phase Infrared Photodissociation Spectroscopy of Cationic Polyaromatic Hydrocarbons. *Astrophys. J.* **2000**, *542*, 404–410.

(12) Lemaire, J.; Boissel, P.; Heninger, M.; Mauclaire, G.; Bellec, G.; Mestdagh, H.; Simon, A.; Caer, S. L.; Ortega, J. M.; Glotin, F.; Maitre, P. Gas Phase Infrared Spectroscopy of Selectively Prepared Ions. *Phys. Rev. Lett.* **2002**, *89* (27), 273002.

(13) Ignasiak, M.; de Oliveira, P.; Levin, C. H.; Scuderi, D. Oxidation of Methionine-Containing Peptides by OH Radicals: Is Sulfoxide the Only Product? Study by Mass Spectrometry and IRMPD Spectroscopy. *Chem. Phys. Lett.* **2013**, *590*, 35–40.

(14) Ignasiak, M.; Scuderi, D.; de Oliveira, P.; Pedzinski, T.; Rayah, Y.; Houée Levin, C. Characterization by Mass Spectrometry and IRMPD Spectroscopy of the Sulfoxide Group in Oxidized Methionine and Related Compounds. *Chem. Phys. Lett.* **2011**, *502* (1), 29–36.

(15) Scuderi, D.; Ignasiak, M. T.; Serfaty, X.; Oliveira, P. de; Levin, C. H. Tandem Mass Spectrometry and Infrared Spectroscopy as a Tool to Identify Peptide Oxidized Residues. *Phys. Chem. Chem. Phys.* **2015**, *17* (39), 25998–26007.

(16) Bergès, J.; Kamar, A.; de Oliveira, P.; Pilmé, J.; Luppi, E.; Houée-Levin, C. Toward an Understanding of the Oxidation Process of Methionine Enkephalin: A Combined Electrochemistry, Quantum Chemistry and Quantum Chemical Topology Analysis. *J. Phys. Chem. B* **2015**, *119* (23), 6885–6893.

(17) Bobrowski, K.; Holcman, J. Formation and Stability of Intramolecular Three-Electron SN, SS, and SO Bonds in One-Electron-Oxidized Simple Methionine Peptides. Pulse Radiolysis. *J. Phys. Chem.* **1989**, *93* (17), 6381–6387.

(18) Bobrowski, K.; Hug, G. L.; Pogocki, D.; Marciniak, B.; Schöneich, C. Stabilization of Sulfide Radical Cations through Complexation with the Peptide Bond: Mechanisms Relevant to Oxidation of Proteins Containing Multiple Methionine Residues. *J. Phys. Chem. B* **2007**, *111* (32), 9608–9620.

(19) Scuderi, D.; Bergès, J.; de Oliveira, P.; Houée-Levin, C. Methionine One-Electron Oxidation: Coherent Contributions from Radiolysis, IRMPD Spectroscopy, DFT Calculations and Electrochemistry. *Radiat. Phys. Chem.* **2016**, *128*, 103–111.

(20) Hug, G. L.; Bobrowski, K.; Pogocki, D.; Hörner, G.; Marciniak, B. Conformational Influence on the Type of Stabilization of Sulfur Radical Cations in Cyclic Peptides. *ChemPhysChem* **2007**, *8* (15), 2202–2210.

(21) Archirel, P.; Bergès, J.; Houée-Lévin, C. Radical Cations of the Monomer and van Der Waals Dimer of a Methionine Residue as Prototypes of (2 Center–3 Electron) SN and SS Bonds. Molecular Simulations of Their Absorption Spectra in Water. *J. Phys. Chem. B* **2016**, *120* (37), 9875–9886.

(22) Pilmé, J.; Luppi, E.; Bergès, J.; Houée-Lévin, C.; de la Lande, A. Topological Analyses of Time-Dependent Electronic Structures: Application to Electron-Transfers in Methionine Enkephalin. *J. Mol. Model.* **2014**, *20* (8), 2368.

(23) Bergès, J.; Domin, D.; Pilmé, J.; Braïda, B.; Houée-Levin, C. •OH Oxidation of Methionine in the Presence of Discrete Water Molecules: DFT, QTAIM and Valence Bond Analyses. *Struct. Chem.* **2020**, *31* (2), 719–730.

(24) Shek, P. Y. I.; Lau, J. K.-C.; Zhao, J.; Grzetic, J.; Verkerk, U. H.; Oomens, J.; Hopkinson, A. C.; Siu, K. W. M. Fragmentations of Protonated Cyclic-Glycylglycine and Cyclic-Alanylalanine. *Int. J. Mass Spectrom.* **2012**, *316–318*, 199–205.

(25) Zou, S.; Oomens, J.; Polfer, N. C. Competition between Diketopiperazine and Oxazolone Formation in Water Loss Products from Protonated ArgGly and GlyArg. *Int. J. Mass Spectrom.* **2012**, *316–318*, 12–17.

(26) Alata, I.; Pérez-Mellor, A.; Ben Nasr, F.; Scuderi, D.; Steinmetz, V.; Gobert, F.; Jaïdane, N.-E.; Zehnacker-Rentien, A. Does the Residues Chirality Modify the Conformation of a

Cyclo-Dipeptide? Vibrational Spectroscopy of Protonated Cyclo-Diphenylalanine in the Gas Phase. *J. Phys. Chem. A* **2017**, *121* (38), 7130–7138.

(27) Oomens, J.; Kempkes, L. J. M.; Geurts, T. P. J.; van Dijk, L.; Martens, J.; Berden, G.; Armentrout, P. B. Water Loss from Protonated XxxSer and XxxThr Dipeptides Gives Oxazoline—Not Oxazolone—Product Ions. *J. Am. Soc. Mass Spectrom.* **2020**, *31* (10), 2111–2123.

(28) Cortes-Clerget, M.; Gager, O.; Monteil, M.; Pirat, J.-L.; Migianu-Griffoni, E.; Deschamp, J.; Lecouvey, M. Novel Easily Recyclable Bifunctional Phosphonic Acid Carrying Tripeptides for the Stereoselective Michael Addition of Aldehydes with Nitroalkenes. *Adv. Synth. Catal.* **2016**, *358* (1), 34–40.

(29) Ueda, T.; Saito, M.; Kato, T.; Izumiya, N. Facile Synthesis of Cyclic Dipeptides and Detection of Racemization. *Bull. Chem. Soc. Jpn.* **1983**, *56* (2), 568–572.

(30) Spinks, J. W. T.; Woods, R. J. *An Introduction to Radiation Chemistry*, 3rd edition.; Wiley-Interscience: New York, 1990.

(31) Kadlcik, V.; Sicard-Roselli, C.; Houée-Levin, C.; Kodicek, M.; Ferreri, C.; Chatgilialoglu, C. Reductive Modification of a Methionine Residue in the Amyloid-β Peptide. *Angew. Chem. Int. Ed.* **2006**, *45* (16), 2595–2598.

(32) Oepts, D.; van der Meer, A. F. G.; van Amersfoort, P. W. The Free-Electron-Laser User Facility FELIX. *Infrared Phys. Technol.* **1995**, *36* (1), 297–308.

(33) Prazeres, R.; Glotin, F.; Insa, C.; Jaroszynski, D. A.; Ortega, J. M. Two-Colour Operation of a Free-Electron Laser and Applications in the Mid-Infrared. *Eur. Phys. J. D* **1998**, *3* (1), 87–93.

(34) Bakker, J. M.; Besson, T.; Lemaire, J.; Scuderi, D.; Maître, P. Gas-Phase Structure of a π-Allyl−Palladium Complex: Efficient Infrared Spectroscopy in a 7 T Fourier Transform Mass Spectrometer. *J. Phys. Chem. A* **2007**, *111* (51), 13415–13424.

(35) Martens, J.; Berden, G.; Gebhardt, C. R.; Oomens, J. Infrared Ion Spectroscopy in a Modified Quadrupole Ion Trap Mass Spectrometer at the FELIX Free Electron Laser Laboratory. *Rev. Sci. Instrum.* **2016**, *87* (10), 103108.

(36) Berden, G.; Derksen, M.; Houthuijs, K. J.; Martens, J.; Oomens, J. An Automatic Variable Laser Attenuator for IRMPD Spectroscopy and Analysis of Power-Dependence in Fragmentation Spectra. *Int. J. Mass Spectrom.* **2019**, *443*, 1–8.

(37) Pracht, P.; Bohle, F.; Grimme, S. Automated Exploration of the Low-Energy Chemical Space with Fast Quantum Chemical Methods. *Phys. Chem. Chem. Phys.* **2020**, *22* (14), 7169–7192.

(38) Conformer-Rotamer Ensemble Sampling Tool Based on the Xtb Semiempirical Extended Tight-Binding Program Package Crest. Https://Github.Com/Grimme-Lab/Crest.

(39) Bannwarth, C.; Ehlert, S.; Grimme, S. GFN2-XTB—An Accurate and Broadly Parametrized Self-Consistent Tight-Binding Quantum Chemical Method with Multipole Electrostatics and Density-Dependent Dispersion Contributions. *J. Chem. Theory Comput.* **2019**, *15* (3), 1652–1671.

(40) Correia, C. F.; Balaj, P. O.; Scuderi, D.; Maitre, P.; Ohanessian, G. Vibrational Signatures of Protonated, Phosphorylated Amino Acids in the Gas Phase. *J. Am. Chem. Soc.* **2008**, *130* (11), 3359–3370.

(41) Paciotti, R.; Coletti, C.; Re, N.; Scuderi, D.; Chiavarino, B.; Fornarini, S.; Crestoni, M. E. Serine O-Sulfation Probed by IRMPD Spectroscopy. *Phys. Chem. Chem. Phys.* **2015**, *17* (39), 25891–25904.

(42) Nei, Y. -w.; Hallowita, N.; Steill, J. D.; Oomens, J.; Rodgers, M. T. Infrared Multiple Photon Dissociation Action Spectroscopy of Deprotonated DNA Mononucleotides: Gas-Phase Conformations and Energetics. *J. Phys. Chem. A* **2013**, *117* (6), 1319–1335.

(43) Frisch, M. J.; Trucks, G. W.; Schlegel, H. B.; Scuseria, G. E.; Robb, M. A.; Cheeseman, J. R.; Scalmani, G.; Barone, V.; Petersson, G. A.; Nakatsuji, H., et al. *Gaussian 16*, Revision B.01; Gaussian, Inc.: Wallingford, CT, 2016.

(44) Neese, F. The ORCA Program System. *WIREs Comput. Mol. Sci.* **2012**, *2* (1), 73–78.

(45) Lioe, H.; O'Hair, R. A. J.; Gronert, S.; Austin, A.; Reid, G. E. Experimental and Theoretical Proton Affinities of Methionine, Methionine Sulfoxide and Their N- and C-Terminal Derivatives. *Int. J. Mass Spectrom.* **2007**, *267* (1), 220–232.

(46) Afonso, C.; Modeste, F.; Breton, P.; Fournier, F.; Tabet, J.-C. Proton Affinities of the Commonly Occuring L-Amino Acids by Using Electrospray Ionization-Ion Trap Mass Spectrometry. *Eur. J. Mass Spectrom.* **2000**, *6* (5), 443–449.

(47) Morsa, D.; Gabelica, V.; Rosu, F.; Oomens, J.; De Pauw, E. Dissociation Pathways of Benzylpyridinium "Thermometer" Ions Depend on the Activation Regime: An IRMPD Spectroscopy Study. *J. Phys. Chem. Lett.* **2014**, *5* (21), 3787–3791.

(48) Piccirillo, S.; Ciavardini, A.; Bodo, E.; Rondino, F.; Scuderi, D.; Steinmetz, V.; Paladini, A. Probing the Competition among Different Coordination Motifs in Metal–Ciprofloxacin Complexes through IRMPD Spectroscopy and DFT Calculations. *Inorg. Chem.* **2013**, *52* (1), 103–112.

(49) Nieuwjaer, N.; Beydoun, A.; Lecomte, F.; Manil, B.; Cappelluti, F.; Guidoni, L.; Scuderi, D.; Desfrançois, C. IRMPD Spectroscopy and Quantum Chemistry Calculations on Mono- and Bi-Metallic Complexes of Acetylacetonate Ligands with Aluminum, Iron, and Ruthenium Ions. *J. Chem. Phys.* **2020**, *153* (23), 234303.

(50) Scuderi, D.; Barbu-Debus, K. L.; Zehnacker, A. The Role of Weak Hydrogen Bonds in Chiral Recognition. *Phys. Chem. Chem. Phys.* **2011**, *13* (40), 17916–17929.

(51) Bakker, J. M.; Sinha, R. K.; Besson, T.; Brugnara, M.; Tosi, P.; Salpin, J.-Y.; Maître, P. Tautomerism of Uracil Probed via Infrared Spectroscopy of Singly Hydrated Protonated Uracil. *J. Phys. Chem. A* **2008**, *112* (48), 12393–12400.

(52) Hiller, K. O.; Masloch, B.; Goebl, M.; Asmus, K. D. Mechanism of the Hydroxyl Radical Induced Oxidation of Methionine in Aqueous Solution. *J. Am. Chem. Soc.* **1981**, *103* (10), 2734–2743.

(53) Gregori, B.; Guidoni, L.; Crestoni, M. E.; de Oliveira, P.; Houée-Levin, C.; Scuderi, D. One-Electron Oxidation of Methionine-Containing Dipeptides of Reverse Sequence: Sulfur

versus Sulfoxide Characterized by IRMPD Spectroscopy and Static and Dynamics DFT Simulations. *J. Phys. Chem. B* **2017**, *121* (9), 2083–2094.

Table 1

	Experiment	Assignment	LLketo01	LLketo02	LLketo04
A	870	νSC, δSCH, δCNH		853	
B	1219	δSCH, δCH_2		1222	1187
C	1315	νCN, νCp-O, δCH_2, δCN(p)H	1323	1287	1306
D	1436	δCH_2, δCN(p)H, νNCα	1433	1433	1445
E	1487	νCpCα, δCN(p)H, δCH_2, δCpOH	1477	1462	
F	1665	νNpC, δCNpH, δCpOH	1653	1633	1672
G	1755	νC=O, δCNH	1734	1746	1737
	Broad band at ca.2600	νOH	2451	2533	
H	2941	νCH_2, νCH_3	2938	2940	2928
		νNpH, $\nu asCH_2$			2981
		νNpH	3053		
		νNpH		3092	
I	3423	νNH	3444	3454	3443
J	3585	νOH			3588

Table 1. Experimental and calculated vibrational frequencies for the selected isomers c(LMetLMet)H^+ at B3LYP/6-311g(d) level of the theory, and corresponding band assignments.

Table 2

	Experiment	Assignment	LLOketo01	LLOketo02	LLOketo03	LLOketo12
A	869	$\nu S{=}OH^+$, δSCH, $\nu S{=}O$	824			927
B	1082	νCN, δSOH, $\nu S{=}O$	1071	1054		1121
C	1181	δCOH, δCH_2, δSOH			1206	1202
D	1289	νCOH, δSOH, δCH_2	1279	1263	1320	1322
E	1427	δNH, δCH_2, δCH_3	1423	1405	1423	1429
F	1592	νCN, νCO, δCNH, δCH_2		1619	1623	
G	1652	$\nu C{=}O$, δCNH	1644			1673
H	1745	$\nu C{=}O$, δCNH	1729	1717	1730	1730
	-	$\nu(S)OH$		2337		2530
I	2938	νCH_2, νCH_3	2934	2928	2933	2933
	Broad band between 2900-3200 cm^{-1}	νNH	3232		3232	
		$\nu(S)OH$	3303			
J	3418	νNH	3431	3421		
K	3497	νNH, νNpH			3438	3450
L	3587	νOH				3545
M	3623	νOH			3596	

Table 2. Experimental and calculated vibrational frequencies for the selected isomers of $[c(LMetLMet)(O)H]^+$ at B3LYP/6-311g(d) level of the theory, and corresponding band assignments.

Table 3

	Experiment	Assignment	LDketo01	LDketo02	LDketo06
A	847	νSC, δCH_2, δCNpH	804		
B	1218	νCpO, δCpOH, νCNp, δCH_2		1167	1206
C	1278	νCN, δCpOH, δCH_2	1250	1276	1266
D	1317	νCpO, νCCα, δCN(p)H	1322	1311	1311
E	1435	$\delta_{scissor}CH_2$,δCH_3, δCN(p)H	1434	1430	1438
F	1495	νCαpCp, δCN(p)H, δCpOH, δCH_2	1493		1471
G	1676	νCNp, δCNpH, δCpOH	1638	1650	1682
H	1751	νC=O, δCNH	1727	1732	1740
I	2942	νCH, νCH_2, νCH_3, νNpH	2936	2934	2926
J	3371	νNpH	3396		
K	3416	νNH	3431		
L	3494	νNH		3446	3447
M	3567	νOH		3579	3602

Table 3. Experimental and calculated vibrational frequencies for the selected isomers of c(LMetDMet)H^+ at B3LYP/6-311g(d) level of the theory, and corresponding band assignments.

Table 4

	Experiment	Assignment	LDOketo 01	LDOketo 02	LDOketo 04	LDOketo06	LDOimin01
A	871	$\nu S{=}OH^+$, $\nu S{=}O$, νCC, δCH_2, δCH_3	814	905	919		
B	1074	$\nu S{=}O$, δCH_2, δCH_3				999	
C	1179	δSCH,$\nu CN(p)$, νCC		1162	1159		1120
D	1281	δSOH, $\nu CN(p)$,$\delta CpOH$, δCH_2	1298	1263	1271	1243	
E	1329	$\nu C(p)O$, $\nu CN(p)$, δCH_2, δCH_3		1322		1320	
F	1425	νCpO, νCN, $\delta CN(p)H$, δCH_2			1412	1431	1428
G	1465	$\nu C\alpha pCp$, $\delta CN(p)H$		1509	1503		
H	1591	$\nu C(p)O$, $\nu CN(p)$, $\delta CN(p)H$	1650	1634	1645		1629/1669
I	1776	$\nu C{=}O$, δCNH, νCNp	1734	1732	1739	1686/1724	
J	2933	νCH_2, νCH_3	2931	2924	2935	2935	2925
	Broad band between 2900 and 3300 cm^{-1}	νNpH			3113		
		$\nu(S)OH$	3196				
K	3412	$\nu N(p)H$	3420	3407			3420
L	3486	νNH		3444	3454	3448	
M	3545	νOH				3559	
N	3579	$\nu(S)OH$					3593

Table 4. Experimental and calculated vibrational frequencies for the selected isomers of $[c(LMetDMet)(O)H]^+$ at B3LYP/6-311g(d) level of the theory, and corresponding band assignments.

Table 5

	Experiment	Assignment	GMketo01	GMketo02	GMketo03	GMketo05
A	879	δSCH, δCNpH		866	870	824
B	1209	δCpOH, νCpO, νCNp	1167	1172	1173	1184
C	1301	δCH_2, δCH_3, νCpO νCαC, νCN	1283	1277	1278	1255
D	1470	δCN(p)H, δCH_2, δCH_3, νCαpCp	1433	1435	1432	1441/1496
E	1639	νCNp, δCNpH	1661	1648	1649	1682
F	1763	νC=O, δCNH	1743	1747	1749	1735
	Broad band between 2600 and 3200 cm^{-1}	νNpH, νCH	2845	2896	2879	
G	2865	νCH_2				2866
H	2944	νCH_2, νCH_3				2934
I	3389	νNpH				3383
J	3416	νNH	3456	3465	3466	3441
K	3564	νOH	3565	3557	3561	
L	3598	νOH				3597

Table 5. Experimental and calculated vibrational frequencies for the selected isomers of $c(GlyMet)H^+$ at B3LYP/6-311g(d) level of the theory, and corresponding band assignments.

Table 6

	Experiment	Assignment	GMOketo01	GMOketo02	GMOketo03
A	881	δSOH, νS=OH$^+$, νS=O, νCC	911	925	919
B	1059	νS=O, νCN(p), νCC, νCpO, δSCH		1077	
C	1152	δSCH,δCpOH, δCH$_2$			1108
D	1212	νCN(p), νCpO, δCOH, δCH$_2$	1251	1190	1200
E	1271	νCN(p), νCCα, δCH$_2$, δCH$_3$	1310		1274
F	1397	νCN(p), δCN(p)H	1384		
G	1446	νC(p)C(αp), δCN(p)H, δCH$_2$	1471	1436	1439
H	1584	νCpCαp, νCNp, δCpOH		1574	
I	1657	νC(p)O, νCN(p), δCN(p)H	1637	1679	
J	1763	νC=O, δCNH	1750	1740	1738
	Broad band between 2600 and 2800 cm^{-1}	νNpH			2678
		ν(S)OH	2763		
K	2931	νCH$_2$	2930	2879	2877
L	3415	νNH	3432	3466	3452
M	3578	νOH		3541	
N	3633	νOH			3606

Table 6. Experimental and calculated vibrational frequencies for the selected isomers of [c(GlyMet(O))H]$^+$ at B3LYP/6-311g(d) level of the theory, and corresponding band assignments.

Figure 1

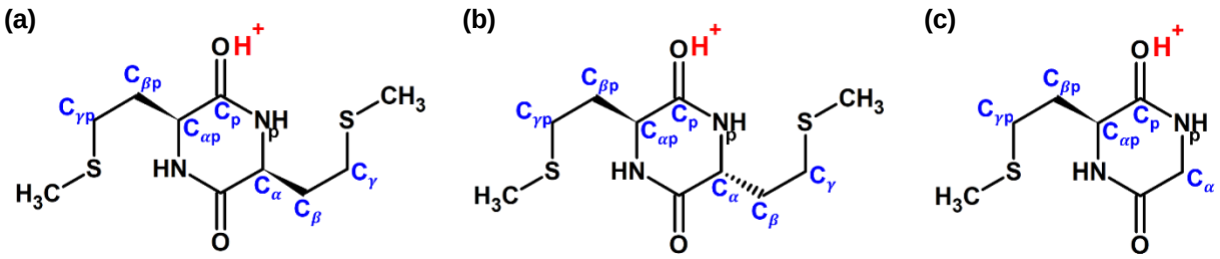

Figure 1. Chemical structures of **(a)** c(LMetLMet)H^+ and **(b)** c(LMetDMet)H^+ and **(c)** c(GlyLMet)H^+, together with the nomenclature used for the atoms in the protonated form on the keto functional group.

Figure 2

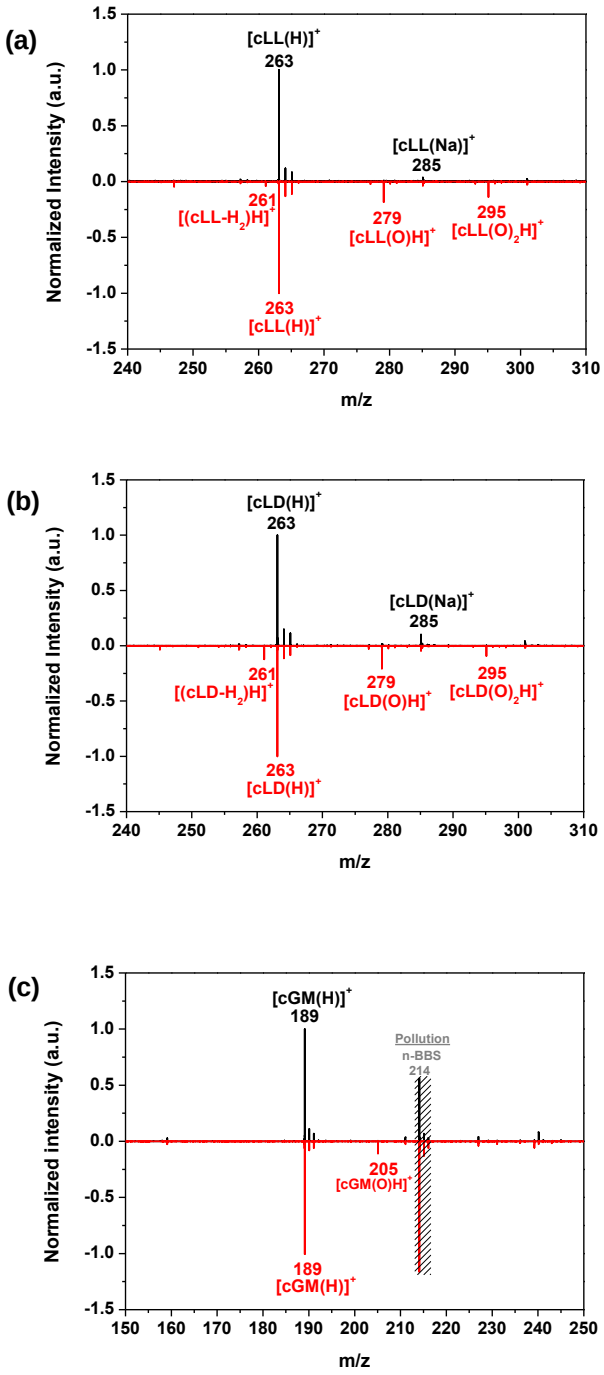

Figure 2. Mass spectra of non-irradiated (black) and irradiated (red) **(a)** c(LMetLMet), referred as $[cLL(H)]^+$ **(b)** c(LMetDMet), referred as $[cLD(H)]^+$ and **(c)** c(GlyMet), referred as $[cGM(H)]^+$ (irradiation dose 833 Gy).

Figure 3

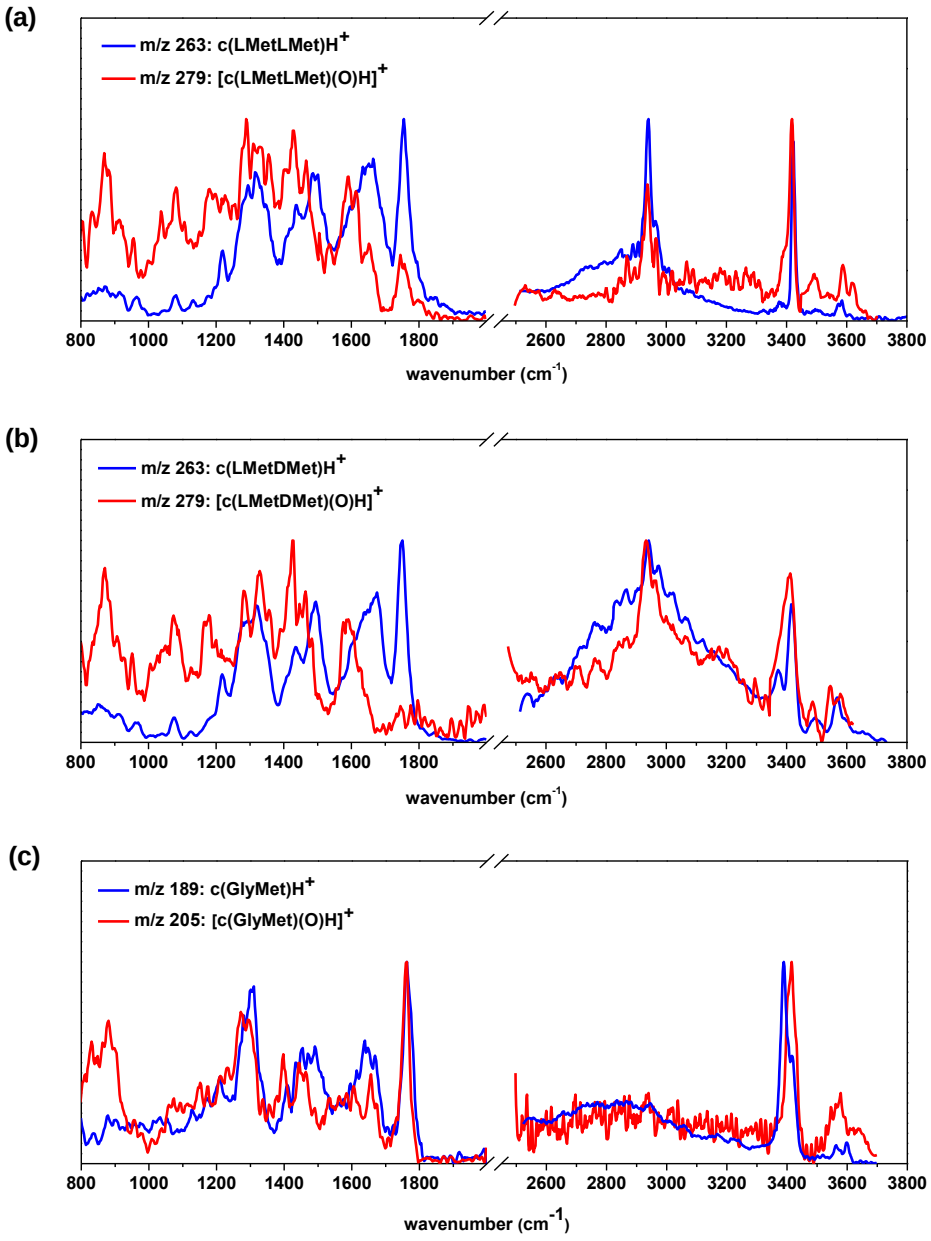

Figure 3. Comparison between the IRMPD spectra of protonated non-oxidized dipeptides (blue) and the ones of protonated singly oxidized molecules (red). **(a)** c(LMetLMet)H^+ and [c(LMetLMet)(O)H]$^+$. **(b)** c(LMetDMet)H^+ and [c(LMetDMet)(O)H]$^+$. **(c)** c(GlyMet)H^+ and [c(GlyMet)(O)H]$^+$.

Figure 4

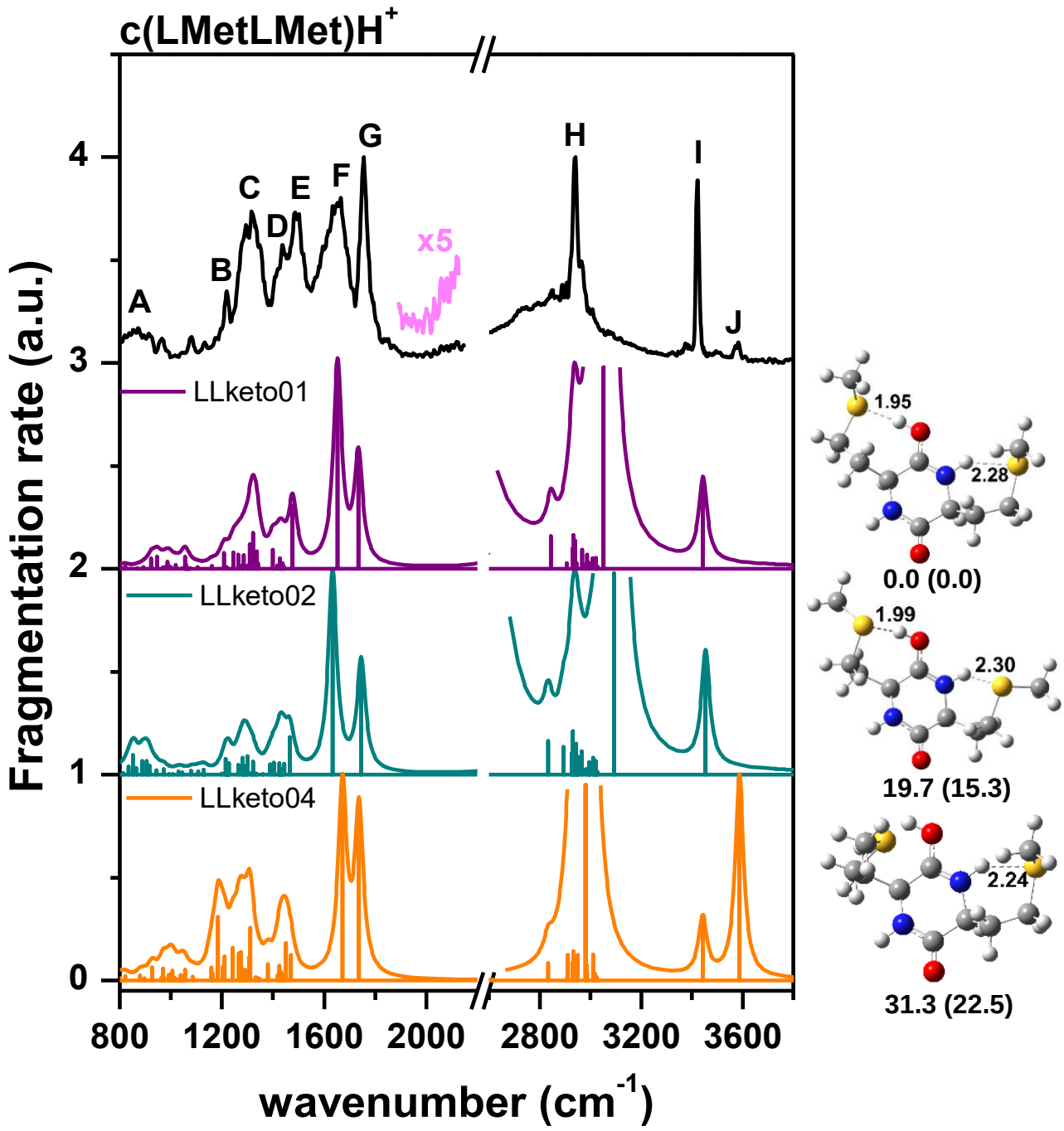

Figure 4. Comparison of the experimental IRMPD spectra of c(LMetLMet)H^+ with convoluted calculated IR absorption spectra of representative conformers of the lowest energies optimized at the B3LYP/6-311g(d) level of theory. The H-bond distances are reported in Å. The corresponding structures are reported on the right together with the relative Gibbs free energy (ΔG) at 298 K in kJ/mol, calculated at B3LYP/6-311g(d) level of theory. Another kind of relative Gibbs free energy in kJ/mol, calculated by a combination of the electronic CCSD(T) energies at the DLPNO-CCSD(T)/cc-pvTZ level of theory with thermal correction (298 K) from the B3LYP/6-311g(d) calculations, is provided in parentheses.

Figure 5

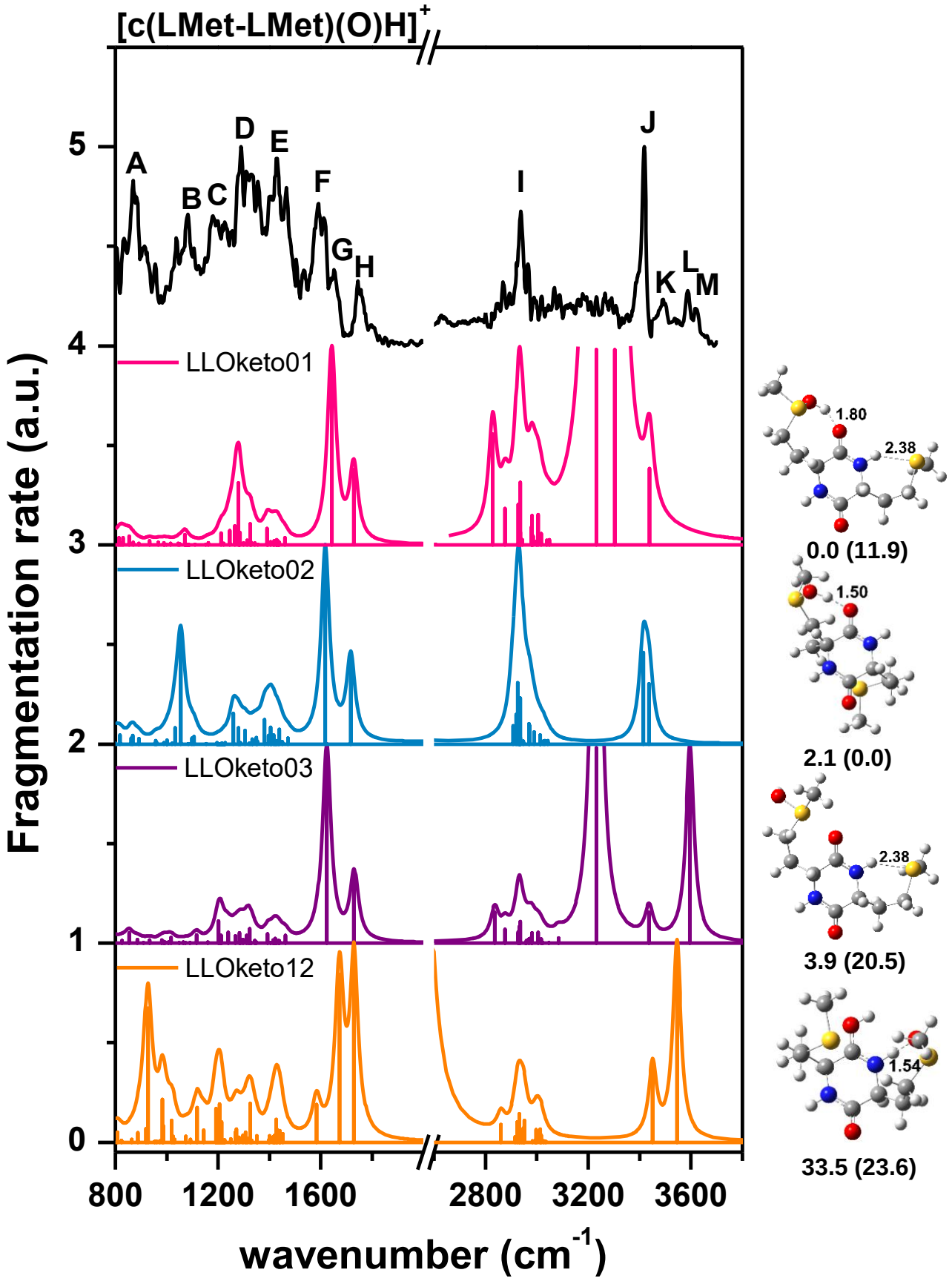

Figure 5. Comparison of the experimental IRMPD spectra of $[c(LMetLMet)(O)H]^+$ with convoluted calculated IR absorption spectra of representative conformers of the lowest energies

optimized at the B3LYP/6-311g(d) level of theory. The H-bond distances are reported in Å. The corresponding structures are reported on the right together with the relative Gibbs free energy (ΔG) at 298 K in kJ/mol, calculated at B3LYP/6-311g(d) level of theory. Another kind of relative Gibbs free energy in kJ/mol, calculated by a combination of the electronic CCSD(T) energies at the DLPNO-CCSD(T)/cc-pvTZ level of theory with thermal correction (298 K) from the B3LYP/6-311g(d) calculations, is provided in parentheses.

Figure 6

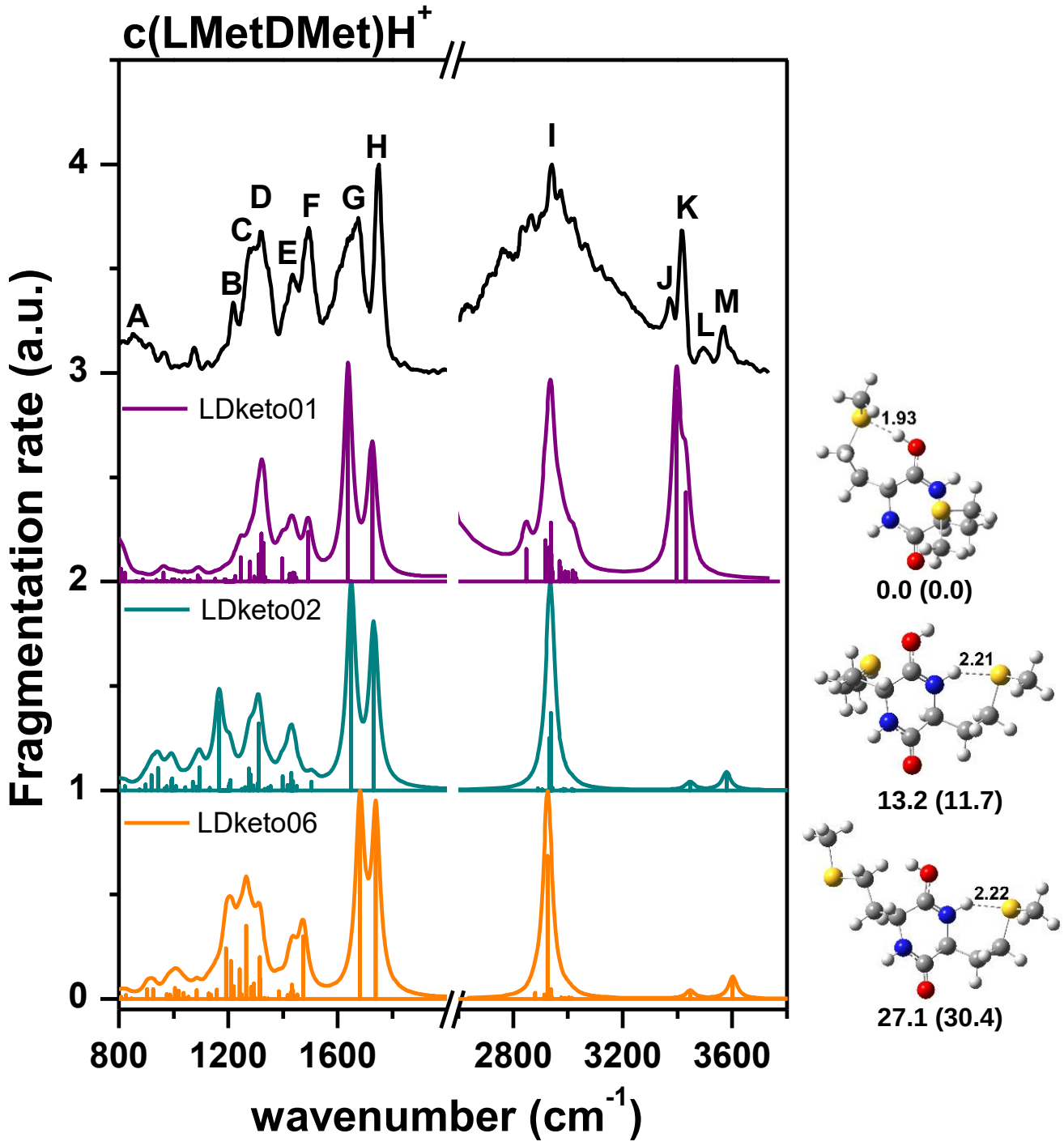

Figure 6. Comparison of the experimental IRMPD spectra of c(LMetDMet)H^+ with convoluted calculated IR absorption spectra of representative conformers of the lowest energies optimized at the B3LYP/6-311g(d) level of theory. The H-bond distances are reported in Å. The corresponding structures are reported on the right together with the relative Gibbs free energy (ΔG) at 298 K in kJ/mol, calculated at B3LYP/6-311g(d) level of theory. Another kind of

relative Gibbs free energy in kJ/mol, calculated by a combination of the electronic CCSD(T) energies at the DLPNO-CCSD(T)/cc-pvTZ level of theory with thermal correction (298 K) from the B3LYP/6-311g(d) calculations, is provided in parentheses.

Figure 7

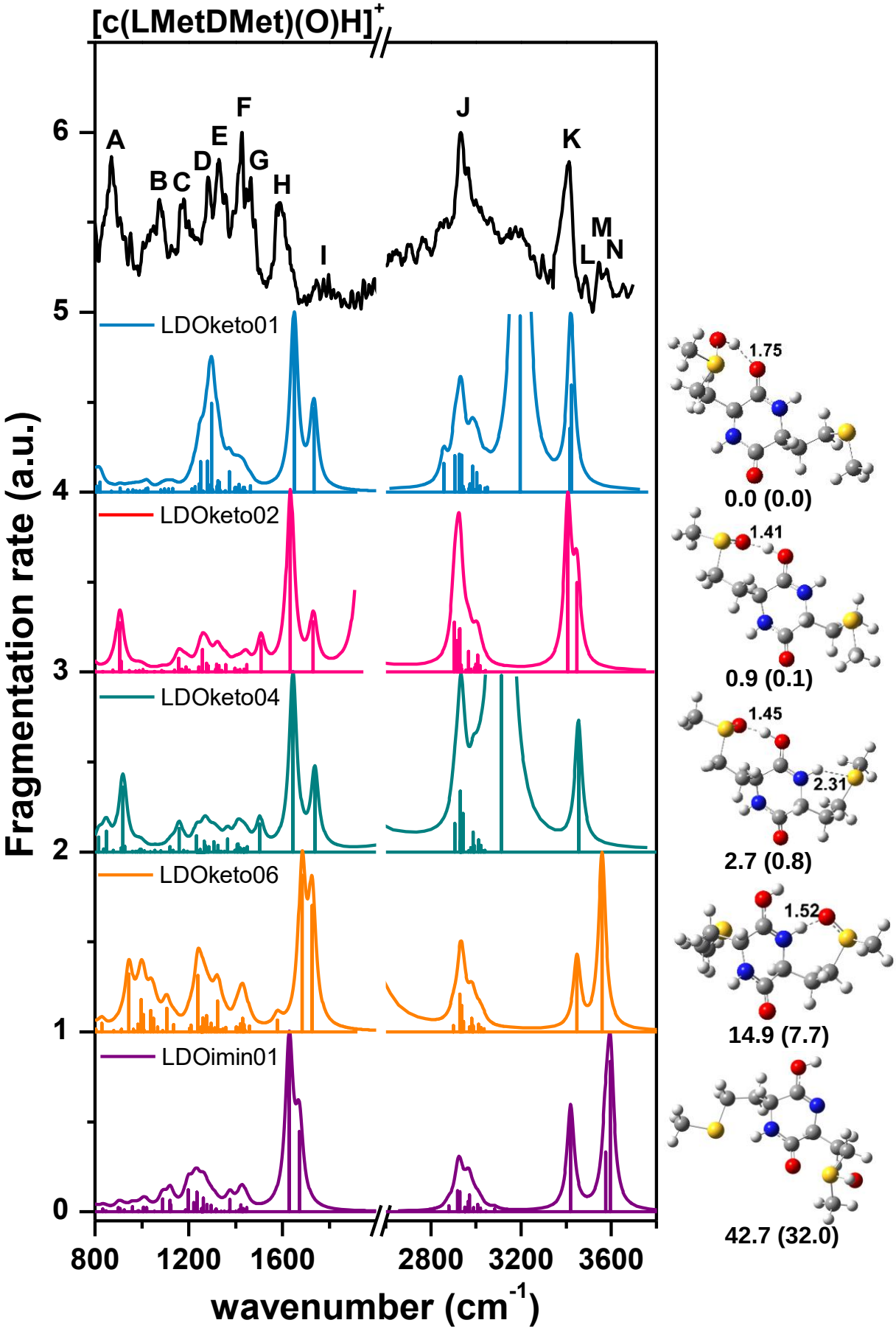
[c(LMetDMet)(O)H]+
A
B C
D
E
F
G
H
I
J
K
L
M
N
LDOketo01
LDOketo02
LDOketo04
LDOketo06
LDOimin01
Fragmentation rate (a.u.)
wavenumber (cm-1)
1.75
0.0 (0.0)
1.41
0.9 (0.1)
1.45
2.31
2.7 (0.8)
1.52
14.9 (7.7)
42.7 (32.0)

Figure 7. Comparison of the experimental IRMPD spectra of [c(LMetDMet)(O)H]$^+$ with convoluted calculated IR absorption spectra of representative conformers of the lowest energies optimized at the B3LYP/6-311g(d) level of theory. The H-bond distances are reported in Å. The corresponding structures are reported on the right together with the relative Gibbs free energy (ΔG) at 298 K in kJ/mol, calculated at B3LYP/6-311g(d) level of theory. Another kind of relative Gibbs free energy in kJ/mol, calculated by a combination of the electronic CCSD(T) energies at the DLPNO-CCSD(T)/cc-pvTZ level of theory with thermal correction (298 K) from the B3LYP/6-311g(d) calculations, is provided in parentheses.

Figure 8

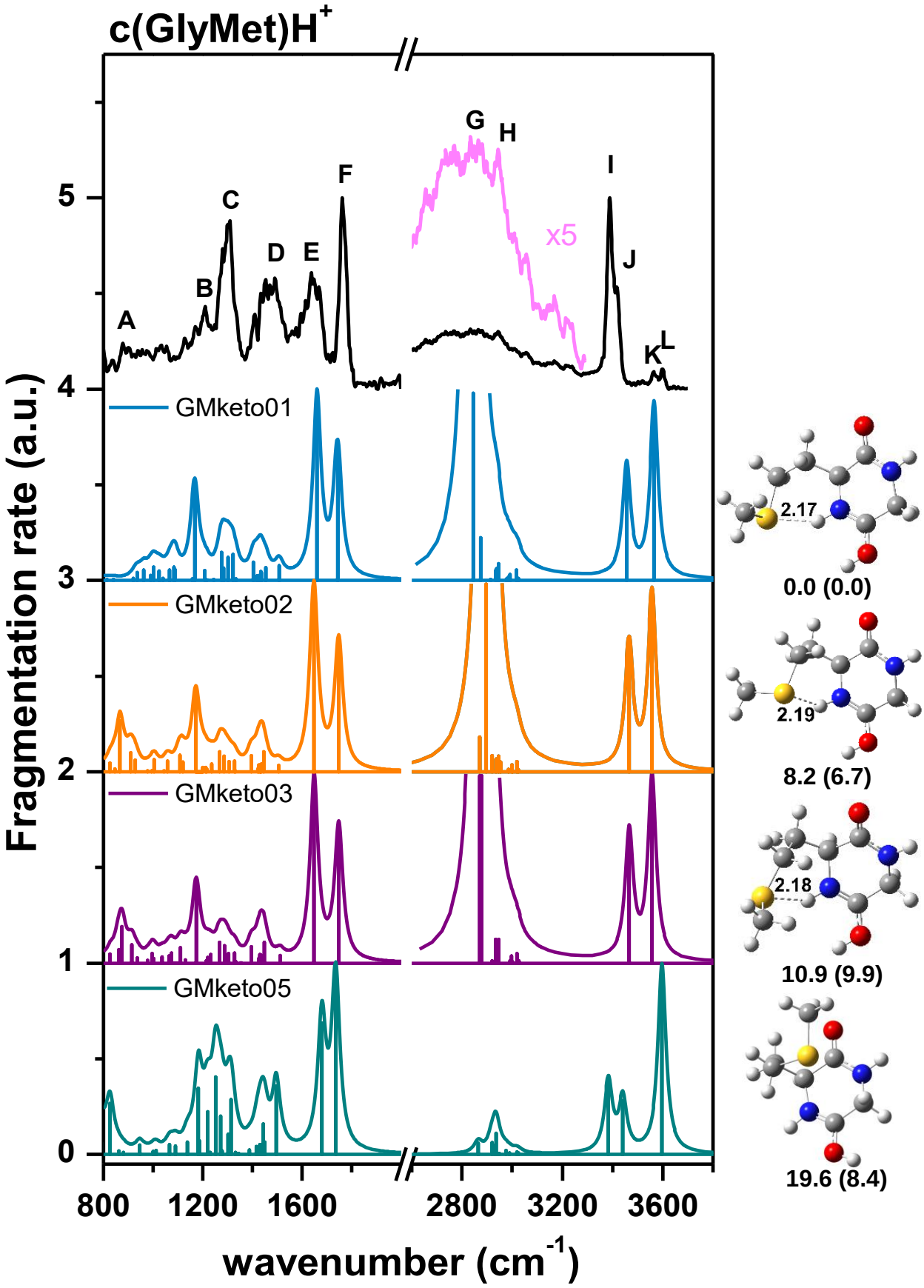
c(GlyMet)H+
A
B
C
D
E
F
G
H
I
J
K
L
x5
GMketo01
GMketo02
GMketo03
GMketo05
Fragmentation rate (a.u.)
wavenumber (cm-1)
2.17
0.0 (0.0)
2.19
8.2 (6.7)
2.18
10.9 (9.9)
19.6 (8.4)

Figure 8. Comparison of the experimental IRMPD spectra of c(GlyMet)H^+ with convoluted calculated IR absorption spectra of representative conformers of the lowest energies optimized at the B3LYP/6-311g(d) level of theory. The H-bond distances are reported in Å. The corresponding structures are reported on the right together with the relative Gibbs free energy (ΔG) at 298 K in kJ/mol, calculated at B3LYP/6-311g(d) level of theory. Another kind of relative Gibbs free energy in kJ/mol, calculated by a combination of the electronic CCSD(T) energies at the DLPNO-CCSD(T)/cc-pvTZ level of theory with thermal correction (298 K) from the B3LYP/6-311g(d) calculations, is provided in parentheses.

Figure 9

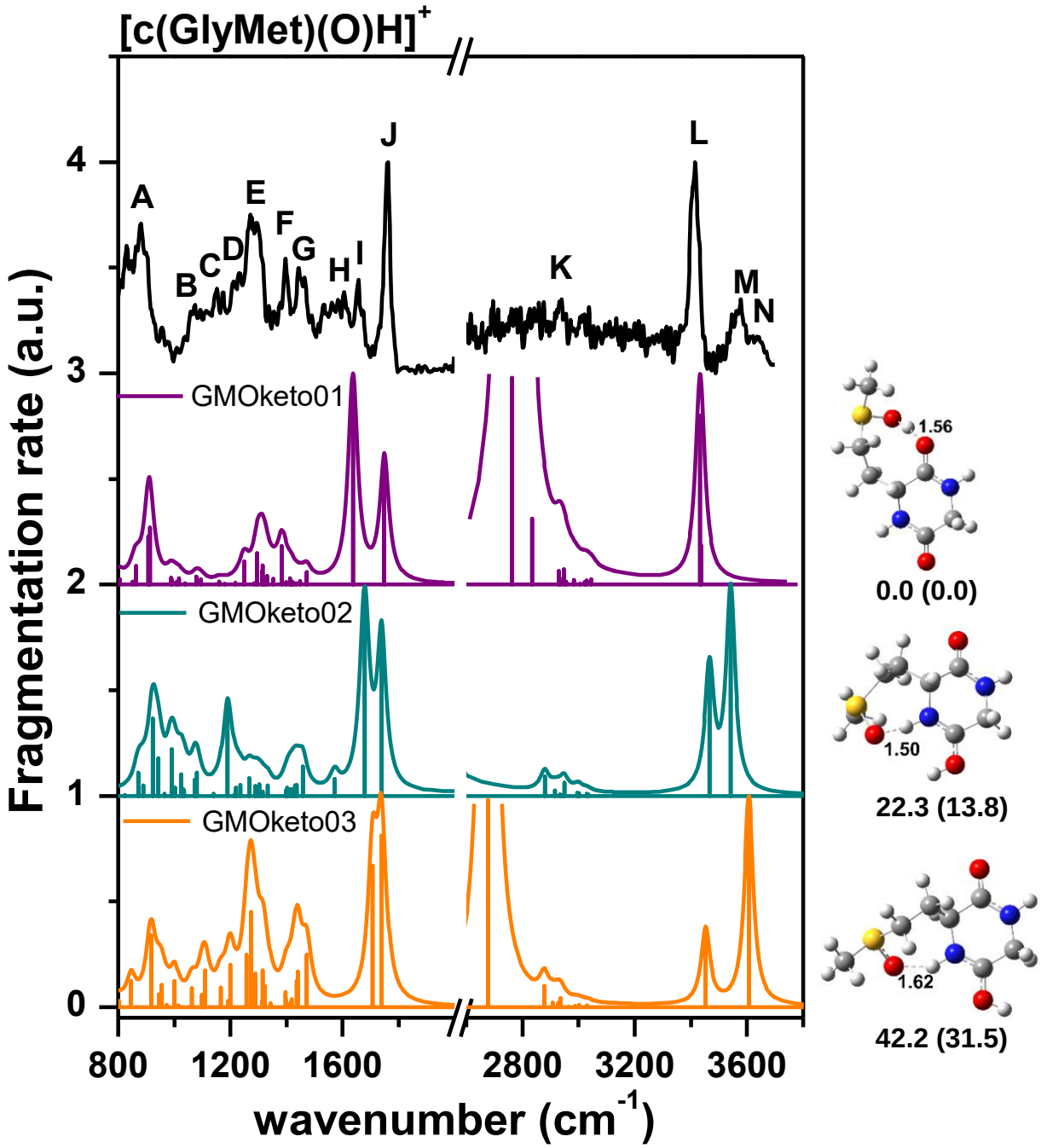

Figure 9. Comparison of the experimental IRMPD spectra of $[c(GlyMet)(O)H]^+$ with convoluted calculated IR absorption spectra of representative conformers of the lowest energies optimized at the B3LYP/6-311g(d) level of theory. The H-bond distances are reported in Å. The corresponding structures are reported on the right together with the relative Gibbs free energy (ΔG) at 298 K in kJ/mol, calculated at B3LYP/6-311g(d) level of theory. Another kind of relative Gibbs free energy in kJ/mol, calculated by a combination of the electronic CCSD(T) energies at the DLPNO-CCSD(T)/cc-pvTZ level of theory with thermal correction (298 K) from the B3LYP/6-311g(d) calculations, is provided in parentheses.

Figure 10

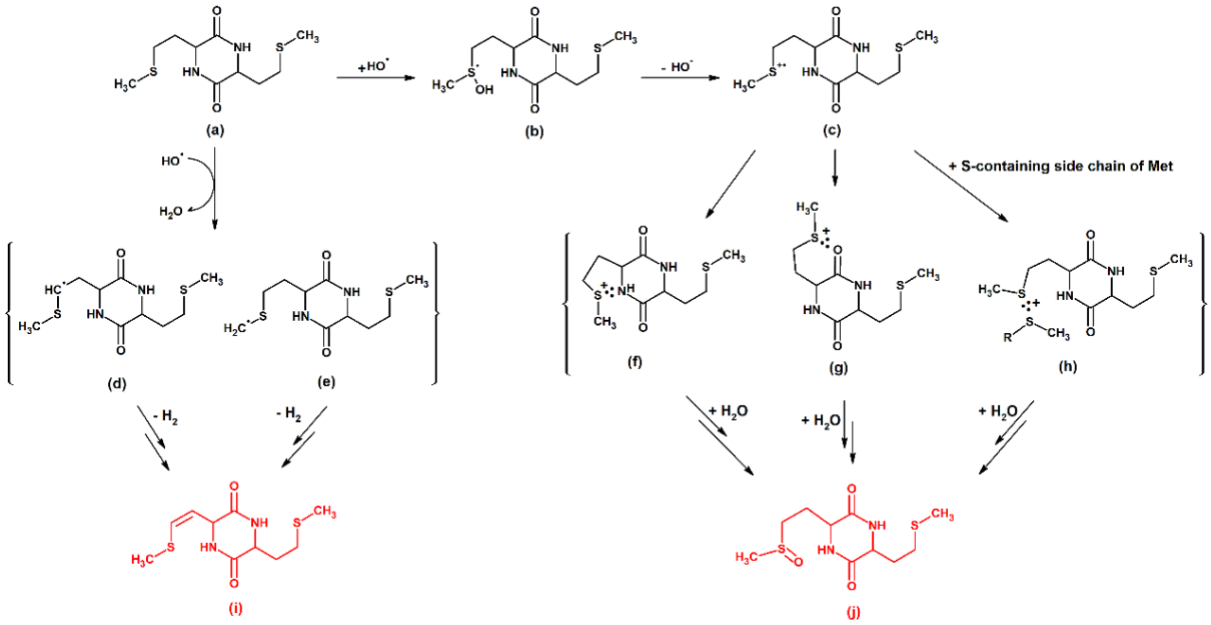

Figure 10. Proposed mechanism of one-electron oxidation in cyclic methionine dipeptide (cMetMet). **(a)** cMetMet. **(b)** Hydroxysulfuranyl radicals (>S•-OH). **(c)** S-centered radical cations (>S•+). **(d)** The α-(alkylthio) radicals (α-S radicals). **(e)** α-S radicals. **(f)** The $(S\therefore N)^+$ intermediates. **(g)** The $(S\therefore O)^+$ intermediates. **(h)** Dimeric radical cations $(S\therefore S)^+$. **(i)** Products from the loss of H_2, [(cMetMet)-H_2]. **(j)** Sulfoxide products, cMetMetSO. Summary of the total mechanisms of one-electron oxidation in cyclic methionine dipeptide are in black (from the review: Houee Levin C.; Bobrowski, K. The use of methods of radiolysis to explore the mechanisms of free radical modifications in proteins. J. Proteom. 2013, 92, 51-61 and references therein). Final oxidation products characterized in this work are highlighted in red.

TOC Graphic

The following graphic will be used for the TOC (8.25 cm x 4.45 cm):